



# Determination of the condensate from optical techniques in unconventional superconductors

C.C. Homes<sup>a,\*</sup>, S. Kamal<sup>b</sup>, D.A. Bonn<sup>b</sup>, R. Liang<sup>b</sup>, W.N. Hardy<sup>b</sup>, B.P. Clayman<sup>c</sup>

<sup>a</sup> Department of Physics, Brookhaven National Laboratory, Upton, NY 11973, USA

<sup>b</sup> Department of Physics and Astronomy, University of British Columbia, Vancouver, British Columbia V6T 1Z1, Canada

<sup>c</sup> Department of Physics, Simon Fraser University, Burnaby, British Columbia V5A 1S6, Canada

Received 11 October 1997; revised 18 October 1997; accepted 10 November 1997

---

## Abstract

The optical properties of superconductors, in particular the real parts of the conductivity and the dielectric function, may be used to calculate the strength of the condensate. In systems where all the free carriers collapse into the condensate, this approach works well. However, in gapless systems, and in unconventional systems in which the superconducting energy gap is observed to have zeros at the Fermi surface, there is usually a considerable amount of residual conductivity at low frequency. This is the case in many of the cuprate-based high-temperature superconductors. In particular,  $\text{YBa}_2\text{Cu}_3\text{O}_{7-\delta}$  is almost perfectly stoichiometric with little chemical disorder ( $\delta \approx 0$ ), yet there is a large amount of residual conductivity both in the copper–oxygen planes as well as perpendicular to the planes for  $T \ll T_c$ , due to the presumed unconventional nature of the energy gap. The assumption that the condensate dominates the optical response at low frequencies leads to optical estimates for the condensate which are too large. However, the microwave surface reactance depends only upon the condensate and is not affected by the presence of residual conductivity (which affects the surface resistance), thus allowing an unambiguous determination of the strength of the condensate. When optical techniques are used in conjunction with microwave techniques, a more complete physical picture emerges. This problem is examined and resolved for the oxygen ‘overdoped’  $\text{YBa}_2\text{Cu}_3\text{O}_{6.99}$  material along the  $c$  axis. © 1998 Elsevier Science B.V.

*Keywords:* Unconventional superconductivity; High- $T_c$  superconductors; Anisotropic; Far infrared; Microwave

---

## 1. Introduction

Infrared techniques have long been acknowledged as a powerful method for probing the electronic properties of metals and superconductors [1]. In particular, optical studies of the cuprate-based high-temperature superconductors have revealed a great deal

of information about the electrodynamics of the normal and superconducting states [2,3].

The optical properties of a material are usually described by complex linear optical response functions, such as the complex dielectric function ( $\tilde{\epsilon}$ ), conductivity ( $\tilde{\sigma}$ ) or index of refraction ( $\tilde{n}$ ). The reflectance of a material is also a complex quantity,  $\tilde{r} = \sqrt{R} e^{i\theta}$ , where  $R = \tilde{r}\tilde{r}^*$  is the reflected intensity and  $\theta$  is the phase difference between the incident and reflected radiation. Normally, only  $R$  is measured in a reflectance experiment. However, if reflectance measurements are performed over a wide

---

\* Corresponding author. Tel.: +1 516 344 7579; Fax: +1 516 344 2739; E-mail: homes@bnl.gov.

enough frequency range the phase may be determined from the Kramers–Kronig relation [4]

$$\theta(\omega) = -\frac{\omega}{\pi} \int_0^{\infty} \frac{\ln[R(\omega')] - \ln[R(\omega)]}{\omega'^2 - \omega^2} d\omega'. \quad (1)$$

Once both the reflectance and phase are known, other optical properties such as  $\tilde{\epsilon}(\omega)$  and  $\tilde{\sigma}(\omega)$  may be calculated [4].

In conventional superconductors, the condensation of the free carriers into a superconducting delta function below  $T_c$  is usually accompanied by the formation of a low-frequency plasma edge in the reflectance. The optical properties of a superconductor can provide an estimate of the strength of the superconducting condensate  $\delta$  ( $\propto \omega_{ps}^2$ ;  $\omega_{ps}^2 = 4\pi n_s e^2/m^*$  is the plasma frequency of the condensate, where  $n_s$  is the density of carriers in the condensate, and  $m^*$  is the effective mass).

The usual technique is to examine the real part of the optical conductivity in the normal state [ $\sigma_{1n}(\omega)$ ] just above  $T_c$ , and well below  $T_c$  [ $\sigma_{1s}(\omega)$ ]. The difference in the conductivities is attributed to the normal-state carriers collapsing into the  $\delta$  function [1]

$$\omega_{ps}^2 = \frac{120}{\pi} \int_0^{\infty} [\sigma_{1n}(\omega) - \sigma_{1s}(\omega)] d\omega. \quad (2)$$

In general, this technique is reliable when the material is a good metal, and when there are no low-lying states. It has been demonstrated that superconductors which contain magnetic impurities [5] have a modified density of states near the energy gap, so that a conventional system can become gapless below the critical value which destroys the superconductivity. These impurities act as strong pair breakers, which results in a substantial amount of residual conductivity below  $T_c$ . On the other hand, unconventional superconductors also display a large amount of residual conductivity below  $T_c$ , even though these systems are essentially free of impurities and disorder [2]. The residual conductivity in these systems is thought to arise from the unconventional nature of the energy gap, which is either highly anisotropic or contains nodes at the Fermi surface [6–9]. This residual conductivity can place an important limitation on optical

conductivity sum rules. For practical reasons, the integral never starts at zero, but at some finite frequency (typically  $\approx 20$ – $50$   $\text{cm}^{-1}$  in most optical experiments). Because a large amount of spectral weight can therefore lie outside the bounds of the integral for both  $\sigma_{1n}(\omega)$  and  $\sigma_{1s}(\omega)$ , significant errors may arise in the estimate of  $\omega_{ps}$ . To try and avoid this problem, a second technique which examines only the superconducting response in the real part of the dielectric function may be used.

If the free carriers in the material that take part in the superconductivity may be described by a Drude model, then the dielectric function ( $\tilde{\epsilon} = \epsilon_1 + i\epsilon_2$ ) for the free carriers may be written as:

$$\tilde{\epsilon}(\omega) = \epsilon_{\infty} - \frac{\omega_{pD}^2}{\omega(\omega + i\Gamma_D)}, \quad (3)$$

where  $\omega_{pD}$  is the Drude plasma frequency, and  $\Gamma_D = 1/\tau$  ( $\tau$  is the scattering rate). If the free carriers are simply ‘Drude-like’ and the scattering-rate is frequency dependent, then a generalized form for the Drude model may be written as

$$\tilde{\epsilon}(\omega) = \epsilon_{\infty} - \frac{\omega_{pD}^2}{\omega[m^*(\omega)/m][\omega + i\Gamma(\omega)]}, \quad (4)$$

where  $\Gamma(\omega) = 1/\tau(\omega)$  and  $m^*(\omega)/m$  describe the frequency-dependent (unrenormalized) carrier scattering rate and effective mass enhancement over the bare (or optical) mass. The effective mass is also given by  $m^*(\omega) = m[1 + \lambda(\omega)]$ , where  $\lambda(\omega)$  is a frequency-dependent renormalization. The complex conductivity is  $\tilde{\sigma}(\omega) = -i\omega\tilde{\epsilon}(\omega)/(4\pi)$ , which neglecting the contributions due to  $\epsilon_{\infty}$ , is  $\tilde{\sigma}(\omega) = \omega_{pD}^2/[4\pi[m^*(\omega)/m][\omega - i\Gamma(\omega)]]$ .

For an appropriate choice of  $\omega_{pD}$ , the  $1/\tau(\omega)$  and  $m^*(\omega)/m$  can be found experimentally by [10]

$$\frac{1}{\tau(\omega)} = \frac{\omega_{pD}^2}{4\pi} \text{Re} \left[ \frac{1}{\tilde{\sigma}(\omega)} \right] \quad (5)$$

and

$$\frac{m^*(\omega)}{m} = \frac{\omega_{pD}^2}{4\pi\omega} \text{Im} \left[ \frac{1}{\tilde{\sigma}(\omega)} \right]. \quad (6)$$

In either the Drude or the generalized-Drude models, in a system where all the free carriers in the normal state have collapsed into the  $\delta$  function [ $\Gamma(\omega \rightarrow 0)$ ]

$= \Gamma_D \approx 0]$ , then for  $T \ll T_c$  the contribution of the condensate to the real part of the dielectric function is [11]

$$\epsilon_1(\omega) = \epsilon_\infty - \frac{\omega_{\text{ps}}^2}{\omega^2}. \quad (7)$$

The value for  $\omega_{\text{ps}}^2$  is determined from a linear regression of  $\epsilon_1(\omega)$  vs.  $\omega^{-2}$  over the low-frequency region. (This is the so-called ‘clean-limit’, where  $\delta \propto \omega_{\text{ps}}^2 \equiv \omega_{\text{pD}}^2$ , for  $T \ll T_c$ .)

Implicit in many of the analysis of high-temperature superconductors is the assumption that  $\delta$  function dominates the optical response at low frequencies, regardless of whether or not all the free carriers have collapsed into the condensate. It is not clear in systems where there is a large amount of residual conductivity that Eq. (2) or Eq. (7) will yield a reliable estimate of  $\omega_{\text{ps}}$ . This is of particular importance when looking at the optical properties of  $\text{YBa}_2\text{Cu}_3\text{O}_{6+x}$  along the  $c$ -axis. In the ‘overdoped’ materials ( $x \approx 1$ ), the anisotropy of this material is significantly lower than in many other cuprate systems [3] and the conductivity takes on a ‘metallic’ character. However, even for  $T \ll T_c$ , there is still a large amount of residual conductivity at low frequency along the  $c$ -axis [12–14], as well as in the planes. To test whether or not optical methods yield reliable estimates for  $\omega_{\text{ps}}$  along the  $c$ -axis, a direct comparison has been made with values for  $\omega_{\text{ps}}$  determined by optical and by microwave techniques.

Microwave techniques are considered to be much more accurate at determining  $\omega_{\text{ps}}$ . While the optical technique is unable to distinguish between the contributions to  $\epsilon_1(\omega)$  or  $\sigma_1(\omega)$  from the condensate and unpaired quasiparticles, the microwave technique probes only the condensate, and thus yields a value for  $\omega_{\text{ps}}$  which is not influenced by the presence of carriers which have not collapsed into the  $\delta$  function. In the limit of local electrodynamics ( $\xi \ll \lambda$ , where  $\xi$  is the coherence length and  $\lambda$  is the London penetration depth), the surface impedance  $Z_s = R_s + iX_s$ , where  $R_s$  is the surface resistance and  $X_s$  is the surface reactance, is related to the complex conductivity ( $\tilde{\sigma} = \sigma_1 + i\sigma_2$ ) by [7]

$$Z_s = \left( \frac{i\mu_0\omega}{\sigma_1 + i\sigma_2} \right)^{1/2}. \quad (8)$$

In the superconducting state at low frequencies ( $\omega\tau \ll 1$ ), the conductivity can be expressed as [7]

$$\tilde{\sigma}(\omega, T) = \sigma_1(\omega, T) + i \frac{1}{\mu_0\omega\lambda^2(T)}. \quad (9)$$

The real part is a measure of the absorption process, both direct electronic excitations and absorption by thermally-activated quasiparticles. The imaginary part is the inductive response of the superconducting condensate. At microwave frequencies in the superconducting state,  $\sigma_2 \gg \sigma_1$  up to temperatures within less than 0.1 K of  $T_c$ . Thus, almost immediately below  $T_c$ , Eqs. (8) and (9) yield simple expressions in the local limit for the surface resistance and surface reactance

$$R_s(T) = \frac{\mu_0^2}{2} \omega^3 \lambda^3(T) \sigma_1(\omega, T) \quad (10)$$

and

$$X_s(T) = \mu_0\omega\lambda(T). \quad (11)$$

Thus, the surface reactance depends only upon the condensate [the penetration depth is related to the plasma frequency of the condensate by  $\lambda^{-1}(T) = 2\pi\omega_{\text{ps}}(T)$ ], and unlike  $R_s$ , is not sensitive upon  $\sigma_1(\omega, T)$  and the presence of any unpaired carriers. (Even if the material is not in the local limit, the microwave technique will still probe only the condensate, although the penetration depth will be more difficult to determine.) This is not the case in either of the optical techniques employed, and thus the microwave method is considered to yield an accurate value for  $\omega_{\text{ps}}$  that will be unaffected by any residual conductivity.

## 2. Experiment

Single crystals of  $\text{YBa}_2\text{Cu}_3\text{O}_{6+x}$  were grown in yttria-stabilized zirconia crucibles using a flux technique [15] and then re-annealed to an oxygen content of  $x \approx 0.99$  ( $T_c \approx 90$  K). The crystals have flat  $ab$ -plane faces, and are typically quite thin ( $\approx 30$   $\mu\text{m}$ ) along the  $c$ -axis. However, crystals with a  $c$ -axis thickness of up to 0.5 mm have been grown.

The reflectance of a  $\text{YBa}_2\text{Cu}_3\text{O}_{6.99}$  crystal with a large  $c$ -axis face ( $\approx 0.5 \times 1.2$  mm) has been mea-

sured from  $\approx 40$  to  $5000 \text{ cm}^{-1}$  using an overfilling technique [16] for the electric field polarized parallel to the  $c$ -axis, above and below  $T_c$ . The optical properties have been calculated from a Kramers–Kronig analysis of the reflectance, which requires extrapolations at high and low frequencies. At low frequency, the reflectance was extrapolated to zero frequency by assuming a Hagen–Rubens  $1 - R \propto \omega^{1/2}$  dependence above  $T_c$ , and  $1 - R \propto \omega^2$  below  $T_c$ . The reflectance has been extended to high frequency ( $\approx 45 \text{ eV}$ ) using the data of Koch et al. [17] and Romberg et al. [18], above which a free-electron behavior ( $R \propto \omega^{-4}$ ) was assumed.

Microwave studies were made using a superconducting split-ring resonator at 1 GHz with  $H_1$  parallel to the  $ab$ -plane of the crystals [6]. As the sample temperature is raised from the base temperature of 1.2 K, the change in field penetration causes the cavity frequency to change. The measurement consists of monitoring the frequency shift  $\Delta f_1(T) \propto a\Delta\lambda_{ab}(T) + c\Delta\lambda_c(T)$ , where  $\Delta\lambda_{ab}(T)$  and  $\Delta\lambda_c(T)$  are the change in the  $ab$ -plane and  $c$ -axis penetration depths from 1.2 K respectively, in a crystal of width  $a$  and thickness  $c$ <sup>1</sup>. Generally, the term involving  $\Delta\lambda_c(T)$  is small and one extracts only  $\Delta\lambda_{ab}(T)$ . However, by making a second measurement after the crystal has been cleaved into  $N$  long platelets, the frequency shift for  $H_1$  parallel to the cleave direction is given by  $\Delta f_2(T) \propto a\Delta\lambda_{ab}(T) + Nc\Delta\lambda_c(T)$ . Comparison of  $\Delta f_1$  and  $\Delta f_2$  allows one to calculate both  $\Delta\lambda_{ab}(T)$  and  $\Delta\lambda_c(T)$  [19]. Normally, this technique can only measure the change of penetration depth from the lowest temperature, 1.2 K. The reason is that one does not know the unloaded frequency of the cavity accurately enough. An exception occurs if the samples are thin enough (less than  $10 \text{ }\mu\text{m}$ ). Then, as the temperature of the crystal is increased well above  $T_c$  into the normal state, the skin depth may become larger than the thickness of the crystal such that the microwave field completely penetrates into the sample. The indication for this situation is no frequency shift as the temperature is further in-

creased. Comparison of the total frequency shifts before and after cleaving the crystal allows a determination of the absolute value of the penetration depth for the  $c$ -axis,  $\lambda_c(0)$ .

### 3. Results and discussion

The reflectance for  $\text{YBa}_2\text{Cu}_3\text{O}_{6.99}$  for  $E\parallel c$  from  $\approx 40$  to  $1000 \text{ cm}^{-1}$  is shown in Fig. 1a for several temperatures above and below  $T_c$ . The reflectance over a wide frequency range is shown in the inset.

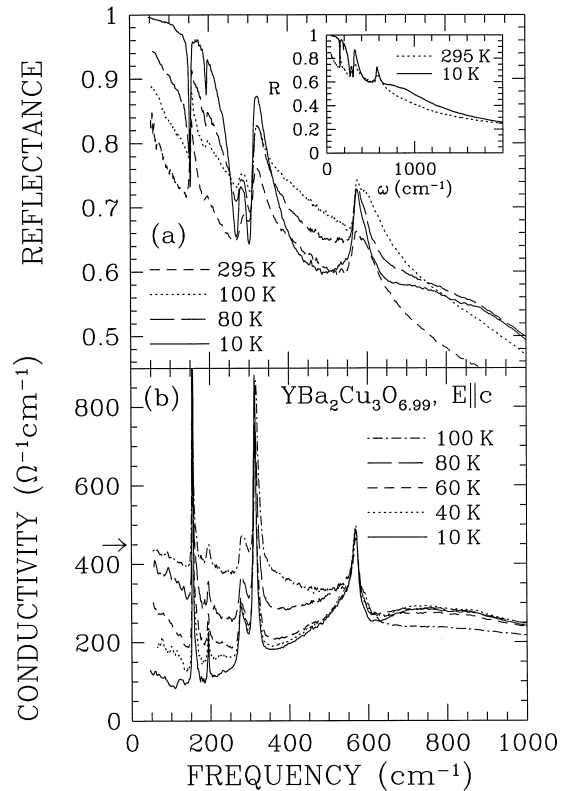


Fig. 1. (a) The reflectance of  $\text{YBa}_2\text{Cu}_3\text{O}_{6.99}$  ( $T_c = 90 \text{ K}$ ), for  $E\parallel c$  from  $\approx 40 \text{ cm}^{-1}$  to  $1000 \text{ cm}^{-1}$  at several temperatures below  $T_c$ , and just above  $T_c$  at 100 K. Inset: the reflectance over a wider frequency range just above  $T_c$  at 100 K, and well below  $T_c$  at 10 K. (b) The real part of the optical conductivity (determined by a Kramers–Kronig analysis of the reflectance curves) for  $E\parallel c$  from  $\approx 40$  to  $1000 \text{ cm}^{-1}$  at 10, 40, 60, 80 and 100 K. The extrapolated value for the DC conductivity just above  $T_c$  at 100 K of  $\approx 450 \text{ }\Omega^{-1} \text{ cm}^{-1}$  is shown by the arrow. Note that even for  $T \ll T_c$  there is still a significant amount of residual conductivity at low frequency.

<sup>1</sup> For the purpose of this measurement the  $ab$ -plane anisotropy is irrelevant. However, the measurements are performed on detwinned crystals in which both  $\Delta\lambda_a(T)$  and  $\Delta\lambda_b(T)$  are measured separately.

The real part of the optical conductivity has been calculated from the reflectance curves and is shown in Fig. 1b for several temperatures below  $T_c$ , and just above  $T_c$  at 100 K. Just above  $T_c$ , the conductivity is characteristic of a poor metal, with an extrapolated value for the DC conductivity of  $\approx 450 \Omega^{-1} \text{ cm}^{-1}$ . Below  $T_c$  the conductivity below  $\approx 500 \text{ cm}^{-1}$  decreases rapidly with decreasing temperature, but even at  $\approx 10 \text{ K}$  there is still a large amount of residual conductivity at low frequency, suggesting that not all of the free carriers have collapsed into the  $\delta$  function.

The optical-conductivity sum rule

$$I(\omega_c) = \frac{120}{\pi} \int_0^{\omega_c} \sigma_1(\omega) d\omega \quad (12)$$

is shown as  $I(\omega)^{1/2}$  for temperatures above  $T_c$  in the normal state, and for  $T \ll T_c$  in the infrared frequency range ( $\omega \leq 1000 \text{ cm}^{-1}$ ) for  $\text{YBa}_2\text{Cu}_3\text{O}_{6.99}$

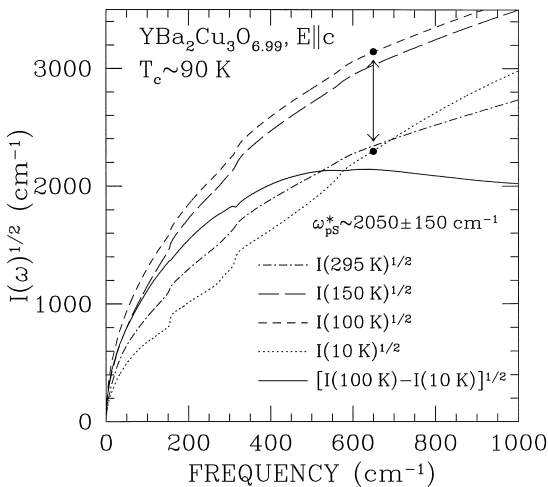


Fig. 2. The integral  $I(\omega)^{1/2}$ , where  $I(\omega) = (120/\pi) \int_0^\omega \sigma_1(\omega') d\omega'$  for  $\text{YBa}_2\text{Cu}_3\text{O}_{6.99}$  along the  $c$ -axis at 295, 150, 100 and 10 K from  $\approx 30$  to  $1000 \text{ cm}^{-1}$ . In the normal state, there is a strong temperature dependence, and  $I(\omega)^{1/2}$  increases rapidly at low frequency with decreasing temperature. The failure of the curves to converge at high frequency also indicates a large amount of temperature dependence in the mid-infrared excitations. Below  $T_c$  for frequencies above  $\approx 400 \text{ cm}^{-1}$ ,  $I(\omega)^{1/2}$  is significantly lower; the difference being attributed to the collapse of the free carriers into  $\omega_{ps}^*$  (solid line), deduced from the sum rule in Eq. (2), yields  $\omega_{ps}^* \approx 2050 \pm 150 \text{ cm}^{-1}$  (where the asterisk denotes an optical result).

along the  $c$ -axis in Fig. 2. In the absence of any bound excitations,  $I(\omega_c \rightarrow \infty)^{1/2} = \omega_{pD}$  for  $T > T_c$ . However, the broad nature of the free-carrier response and the presence of bound excitations in the mid infrared makes any determination of  $\omega_{pD}$  very sensitive upon the choice of  $\omega_c$ .

In the normal state, the rapid increase in  $I(\omega)^{1/2}$  at low frequency is an indication that the spectral weight associated with the free carriers has shifted to low frequency. Below  $T_c$ ,  $I(\omega)^{1/2}$  at 10 K is now considerably less than the 100 K curve, and for  $\omega \geq 400 \text{ cm}^{-1}$  the two curves appear to be offset by a constant amount; the difference between  $I(\omega)^{1/2}$  for  $T \geq T_c$  and  $T \ll T_c$  is attributed to the collapse of the free carriers into the superconducting condensate. The strength of the condensate can be calculated from the optical-conductivity sum rule in Eq. (2), and is shown by the solid line in Fig. 2. Note that above  $\approx 400 \text{ cm}^{-1}$ ,  $\omega_{ps}^* \approx 2050 \pm 150 \text{ cm}^{-1}$  (the asterisk denotes the optically-determined value). As previously noted, the practical lower limit of the integral is  $\approx 40 \text{ cm}^{-1}$ , so that if there is a large amount of spectral weight below  $\approx 40 \text{ cm}^{-1}$  for  $\sigma_1(\omega)$ , either in the normal state or below  $T_c$ , then significant errors may arise.

The real part of the dielectric function is shown in Fig. 3 below  $800 \text{ cm}^{-1}$  at 10 K. The reduced free-carrier response along the  $c$ -axis results in a much stronger phonon spectrum. However, the nearly stoichiometric nature of this material and lack of chemical disorder results in modes with symmetric line shapes and narrow line widths (with the exception of the  $570 \text{ cm}^{-1}$  mode, which is slightly asymmetric). These line shapes are considerably simpler than in the 'underdoped' materials ( $\text{YBa}_2\text{Cu}_3\text{O}_{6+x}$ , for  $x \leq 0.9$ ) [20]. A modified Lorentz model was used to fit the phonons to  $\sigma_1(\omega)$ , and subsequently subtract the phonon contribution  $\tilde{\epsilon}_{ph}(\omega)$  from  $\tilde{\epsilon}_1(\omega)$ , where

$$\tilde{\epsilon}_{ph}(\omega) = \sum_j \frac{\omega_{pj}^2 e^{i\theta_j}}{\omega_{TO,j}^2 - \omega^2 + i\omega\gamma_j}, \quad (13)$$

where  $\omega_{TO,j}$ ,  $\gamma_j$ , and  $\omega_{pj}$  are the frequency, width and effective plasma frequency of the  $j$ -th phonon;  $\theta_j$  is a phase angle to model asymmetric line

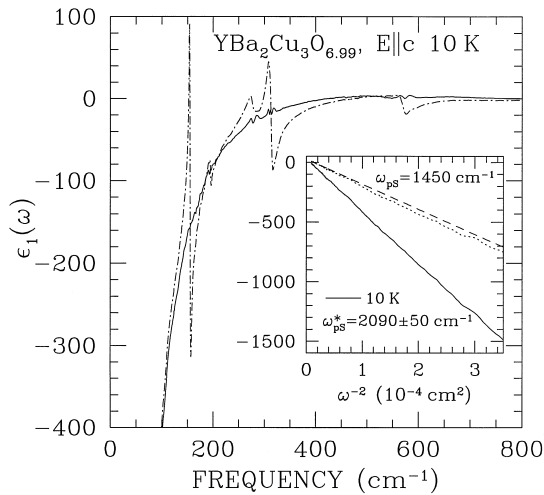


Fig. 3. The real part of the dielectric function  $\epsilon_1(\omega)$  of  $\text{YBa}_2\text{Cu}_3\text{O}_{6.99}$  for  $E\parallel c$  from  $\approx 40$  to  $800\text{ cm}^{-1}$  at 10 K with the phonons present (dash-dot line) and removed (solid line). Inset:  $\epsilon_1(\omega)$  with the phonons removed vs.  $\omega^{-2}$  from  $\approx 50$  to  $500\text{ cm}^{-1}$  (solid line). The value for  $\omega_{\text{ps}}^* = 2090 \pm 70\text{ cm}^{-1}$  at 10 K has been determined from a linear regression of  $\epsilon_1(\omega)$  over the same frequency range. The slope that would be required to give a value of  $\omega_{\text{ps}} = 1450\text{ cm}^{-1}$  (as determined by microwave techniques) is shown by the dashed line. The difference between these two lines is the contribution to  $\epsilon_1(\omega)$  due to the unpaired free carriers (dotted line).

shapes<sup>2</sup>. The real part of the dielectric function with the phonons subtracted is shown in Fig. 3. The inset in Fig. 3 shows  $\epsilon_1(\omega)$  vs.  $\omega^{-2}$  at 10 K, which shows a strong linear behavior. From Eq. (7), the linear regression of  $\epsilon_1(\omega)$  vs.  $\omega^{-2}$  yields the square of the plasma frequency of condensate  $\omega_{\text{ps}}^2$ , or  $\omega_{\text{ps}}^* = 2090 \pm 70\text{ cm}^{-1}$  at  $\approx 10\text{ K}$ . The values for  $\omega_{\text{ps}}^*$  determined from the optical-conductivity sum rule, and from an analysis of  $\epsilon_1(\omega)$  are nearly identical. From  $\lambda^{-1}(T) = 2\pi\omega_{\text{ps}}(T)$ , the penetration depth along the  $c$ -axis is then  $\approx 7800\text{ \AA}$  at  $\approx 10\text{ K}$ .

However, microwave measurements made at 1 GHz on a sample with the same oxygen stoichiometry yield  $\lambda_c \approx 11000\text{ \AA}$ , or  $\omega_{\text{ps}} = 1450 \pm 50\text{ cm}^{-1}$

at 1.2 K. The microwave value for the plasma frequency of the condensate is considerably less than the optically-determined value, and due to the presence of residual conductivity below  $T_c$ , is considered to be the more accurate value (as noted in the introduction).

Using Eq. (7) and the microwave value for  $\omega_{\text{ps}}$ , the additive nature of the terms in the dielectric function allows the contribution to  $\epsilon_1(\omega)$  due to the condensate to be removed, resulting in the dashed and dotted lines in the inset in Fig. 3, respectively. The resulting value for  $\epsilon_1(\omega)$  is still quite large at low frequency, and is in agreement with the large amount of residual conductivity along the  $c$ -axis in Fig. 1b; this residual conductivity has also been observed in other works [12–14], and indicates that a large number of the normal-state free carriers remain unpaired below  $T_c$ . This is not consistent with the ‘clean limit’ picture in which all the free carriers collapse into the  $\delta$  function, and thus Eq. (7) should be rewritten as

$$\epsilon_1(\omega) = \epsilon_\infty - \frac{\omega_{\text{pD}}^2}{\omega^2} \times \left\{ x_s + x_n \left( \frac{\omega^2}{[m^*(\omega)/m][\omega^2 + \Gamma(\omega)^2]} \right) \right\}, \quad (14)$$

where it has been assumed for simplicity that the effective mass enhancement of the condensate is unity. Adopting the language of the two-fluid model [21], the superfluid fraction  $x_s = (\omega_{\text{ps}}/\omega_{\text{pD}})^2$ , and the normal-fluid fraction is  $x_n = (\omega_{\text{pN}}/\omega_{\text{pD}})^2$ , where  $\omega_{\text{pN}}$  is the plasma frequency of the normal-fluid component. The condition that  $x_n + x_s = 1$  requires that  $\omega_{\text{pN}}^2 + \omega_{\text{ps}}^2 = \omega_{\text{pD}}^2$ .

The action of removing the condensate from the dielectric function to give the contribution due to the unpaired carriers yields a result, which when plotted in the manner shown in the inset in Fig. 3 (dotted line), is still surprisingly linear. It is important to consider under what conditions the normal-state carriers can produce a behavior in  $\epsilon_1(\omega)$  similar to that of a condensate. Fig. 4 shows  $\epsilon_1(\omega)$  vs.  $\omega^{-2}$  for a Drude model using  $\omega_{\text{pD}} = 1500\text{ cm}^{-1}$  for  $\omega$  from 50 to  $800\text{ cm}^{-1}$ , with values of  $\Gamma_{\text{D}}$  from 0 to  $100\text{ cm}^{-1}$ . For values of  $\Gamma_{\text{D}} \lesssim 20\text{ cm}^{-1}$ , the resulting

<sup>2</sup> Five phonons were fitted to the optical conductivity at 10 K, the returned parameters are:  $\omega_{\text{TO},1} = 155.2$ ,  $\gamma_1 = 2.7$ ,  $\omega_{\text{p1}} = 412$ ;  $\omega_{\text{TO},2} = 194.3$ ,  $\gamma_2 = 2.8$ ,  $\omega_{\text{p2}} = 141$ ;  $\omega_{\text{TO},3} = 279.0$ ,  $\gamma_3 = 17.6$ ,  $\omega_{\text{p3}} = 391$ ;  $\omega_{\text{TO},4} = 312.7$ ,  $\gamma_4 = 8.6$ ,  $\omega_{\text{p4}} = 603$ ;  $\omega_{\text{TO},5} = 571.6$ ,  $\gamma_5 = 23.5$ ,  $\omega_{\text{p5}} = 566$ . All units are in  $\text{cm}^{-1}$ . All rotation angles are in radians,  $\theta_{1-4} = 0$ , and  $\theta_5 = -0.53$  rads.

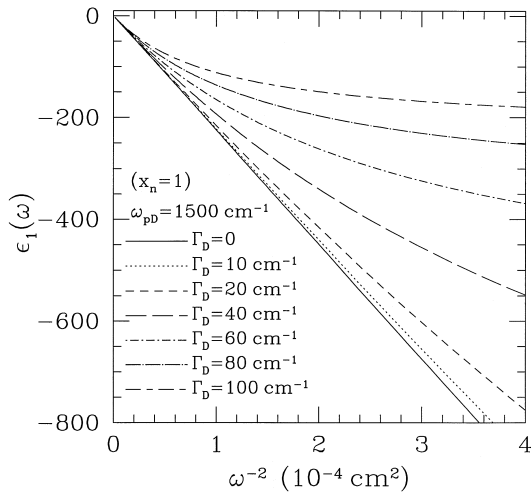


Fig. 4. The real part of the dielectric function vs.  $\omega^{-2}$  for  $\omega_{pD} = 1500 \text{ cm}^{-1}$  for  $\omega$  from 50 to  $800 \text{ cm}^{-1}$ , with various values of  $\Gamma_D$ , as determined using the Drude model (Eq. (3)). When  $\omega \gg \Gamma_D$ , the curves have a strong linear character. However, for larger values of  $\Gamma_D$ , the curves are nonlinear. A linear regression of the  $\Gamma_D = 0 \text{ cm}^{-1}$  curve yields  $\omega_{pD} = 1500 \text{ cm}^{-1}$ ; other regressions yield values for  $\omega_{pD}$  of 1480, 1425, 1260, 1090, 930 and  $800 \text{ cm}^{-1}$  for increasing values of  $\Gamma_D$ , respectively.

lines have a strong linear character, while larger values of  $\Gamma_D$  produce a non-linear behavior. Because the lowest frequency shown in Fig. 4 is  $50 \text{ cm}^{-1}$ , a general conclusion is that if  $\omega \gg \Gamma_D$  then  $\epsilon_1(\omega)$  vs.  $\omega^{-2}$  will be linear. This result also comes directly from Eq. (14), when  $x_s = 0$  and  $x_n = 1$ ; for  $\omega \gg \Gamma_D$  then  $\epsilon_1(\omega) \approx \epsilon_\infty - \omega_{pD}^2/\omega^2$ , so that the slope for the smallest values of  $\Gamma_D$  in Fig. 4 is approximately  $\omega_{pD}$ . Thus, a linear regression of the residual component in  $\epsilon_1(\omega)$  shown in the inset of Fig. 3 yields a value of  $\omega_{pN} = 1500 \pm 50 \text{ cm}^{-1}$ . Using  $\omega_{pD}^2 = \omega_{pN}^2 + \omega_{pS}^2$ , then one can estimate that  $\omega_{pD} = 2100 \pm 70 \text{ cm}^{-1}$ . Of course, this value of  $\omega_{pD}$  is just  $\omega_{pS}$ , as the linear regression of  $\epsilon_1(\omega)$  in Fig. 3 does not distinguish between the condensate and a narrow residual component. The general result that  $\Gamma_D$  is small (less than the lowest measured frequency) when  $T \ll T_c$  indicates that a detailed knowledge of the scattering rate is not necessary. The values for  $\omega_{pS}$  and  $\omega_{pD}$  along the  $c$ -axis indicate that  $\approx 50\%$  of the free carriers have collapsed into the condensate, which is qualitatively similar to what is observed in the  $ab$ -plane [10].

The experimentally-determined value for  $\omega_{pD} \approx 2100 \text{ cm}^{-1}$  is considerably lower than previous estimates of  $\omega_{pD} \approx 4000\text{--}5000 \text{ cm}^{-1}$  [12–14,22]. However, it should be noted that the larger values cited were obtained using a two-component Drude–Lorentz fit [2] to the optical conductivity just above  $T_c$ . The application of the two-component model requires the addition of a number of arbitrary oscillators to account for the conductivity in the mid-infrared region, thus the result for  $\omega_{pD}$  may have large errors associated with it. It is important to establish that the value for  $\omega_{pD}$  along the  $c$ -axis determined for  $\text{YBa}_2\text{Cu}_3\text{O}_{6.99}$  in this work is accurate. The self-consistency of the value of  $\omega_{pD}$  may be established by looking at the relationship between  $1/\tau(\omega)$  and the predicted residual conductivity. The frequency-dependent scattering rate is shown in Fig. 5a for several different values of  $\omega_{pD}$  with the phonons subtracted from the data using the previously described method; choosing different values of  $\omega_{pD}$  in Eqs. (5) and (6) simply scales the results for  $1/\tau(\omega)$  and  $m^*(\omega)/m$ , respectively. The complex dielectric function may then be calculated from Eq. (4), and the predicted value for  $\sigma_1(\omega)$  (the residual component of the conductivity) is shown in Fig. 5b. From Fig. 1b, the observed value of the residual conductivity is  $\approx 100 \Omega^{-1} \text{ cm}^{-1}$  below about  $200 \text{ cm}^{-1}$ , which corresponds to the calculated conductivity in Fig. 5b using the experimentally determined value of  $\omega_{pD} \approx 2000 \text{ cm}^{-1}$ , demonstrating the self-consistency of this result. The larger values of  $\omega_{pD}$  that have been previously observed yield values for the residual component of the conductivity that are much larger than what is actually observed in this work.

An accurate value for  $\omega_{pD}$  along the  $c$ -axis is important in estimating the normal-state anisotropy. Since the classical plasma frequency is  $\omega_{pD}^2 = 4\pi ne^2/m^*$ , where  $n$  is the carrier density and  $m^*$  is the effective mass, then  $(\omega_{p,\parallel}/\omega_{p,\perp})^2 = m_\perp^*/m_\parallel^*$  is an estimate of the mass anisotropy. In this case  $\omega_{p,\parallel}$  and  $\omega_{p,\perp}$  are the normal-state Drude plasma frequencies of the free carriers in the copper–oxygen planes (along the  $a$ -axis), and perpendicular to the planes (along the  $c$ -axis), respectively. Taking  $\omega_{p,\parallel} \approx 15000 \text{ cm}^{-1}$  [23], and  $\omega_{p,\perp} = 2100 \text{ cm}^{-1}$  yields  $m_\perp^*/m_\parallel^* \approx 50$  in the normal state, which is larger than previous estimates [13]. The anisotropy in the superconducting state for  $T \ll T_c$  is estimated from

the ratio of the penetration depths,  $(\lambda_{\perp}/\lambda_{\parallel})^2$ . Using  $\lambda_{\parallel} \approx 1500 \text{ \AA}$  [24,25], and  $\lambda_{\perp} \approx 11\,000 \text{ \AA}$  from the microwave measurements [26], then  $(\lambda_{\perp}/\lambda_{\parallel})^2 \approx 50$ , indicating that the anisotropy has not changed below  $T_c$ . This result contrasts with previous estimates which had the anisotropy increasing by nearly an order of magnitude below  $T_c$ . The previous overestimates of the increase in anisotropy below  $T_c$  arose mainly from the overestimates of  $\omega_{pD}$  along the  $c$ -axis, which lead to underestimates of the anisotropy in the normal state.

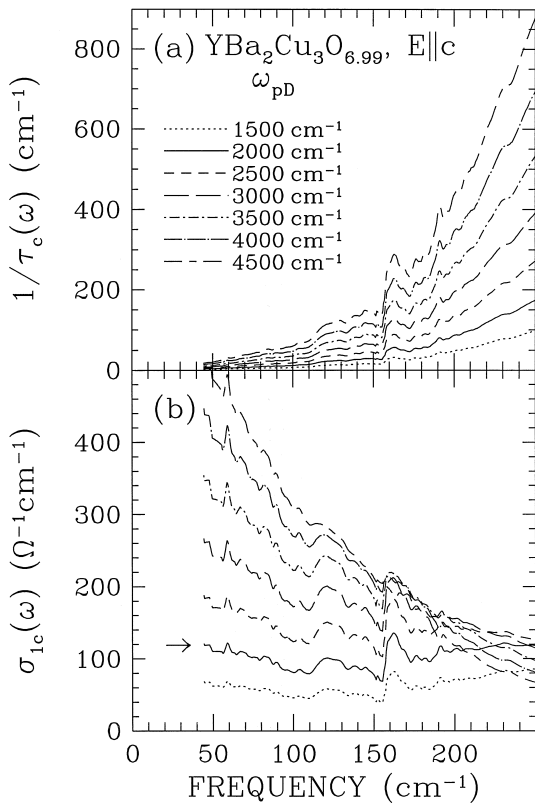


Fig. 5. (a) The experimentally-determined frequency-dependent scattering rate  $1/\tau(\omega)$  (with the phonons removed) for several different choices of the Drude plasma frequency,  $\omega_{pD}$ . Note that the results scale linearly with  $\omega_{pD}$ . (b) The calculated optical conductivity  $\sigma_1(\omega)$  (with the phonons removed), based on the experimentally-determined values of  $1/\tau(\omega)$  and  $m^*(\omega)/m$  for the different choices of  $\omega_{pD}$  in the upper panel. Note that the choice of  $\omega_{pD} = 2000 \text{ cm}^{-1}$  (close to the experimentally-determined value of  $\omega_{pD} \approx 2100 \text{ cm}^{-1}$ ) yields approximately the same value for the residual component of the conductivity at low frequency as is observed experimentally in Fig. 1b.

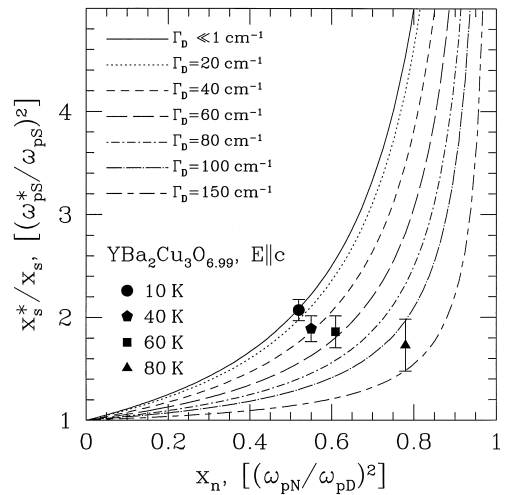


Fig. 6. The resulting overestimate of the superfluid fraction, expressed as the ratio of  $x_s^*/x_s$ , where  $x_s^*$  is the optically-determined value for the superfluid fraction [from a linear regression of  $\epsilon_1(\omega)$  vs.  $\omega^{-2}$ ], and  $x_s$  is the true value of the superfluid fraction, as a function of  $x_n$  for several (constant) values of  $\Gamma_D$ . (These curves are valid for any choice of  $\omega_{pD}$ .) The dots denote the experimentally-determined values of  $x_s^*/x_s$  vs.  $x_n$  for  $\text{YBa}_2\text{Cu}_3\text{O}_{6.99}$  with  $E \parallel c$  for  $T < T_c$ .

The conclusion that the presence of a normal-state component with a ‘narrow’ damping below  $T_c$  can lead to overestimates of  $\omega_{pS}$  can be generalized using Eq. (14). Fig. 6 shows the resulting overestimate of the superfluid fraction, expressed as a ratio of  $x_s^*/x_s$  for different values of  $x_n$  and  $\Gamma_D$ . [For simplicity, it has been assumed that  $\Gamma(\omega) \approx \Gamma_D$  over the frequency range of interest, and that  $\Gamma_D$  is small.] The value of  $x_s^*$  has been determined numerically from a linear regression of the real part of the dielectric function in Eq. (14)<sup>3</sup>. Note that the family of lines depends upon the absolute value of  $\Gamma_D$  rather than a normalized value. Given that  $x_s^*/x_s \approx 2$  in the present case, then if  $\Gamma_D$  is small one immediately has that  $x_n \approx 0.5$ , which is in good agreement with the previous result. This suggests that for  $T \ll$

<sup>3</sup> The frequency range for the linear regression of  $\epsilon_1(\omega)$  vs.  $\omega^{-2}$  from Eq. (6) has been chosen to be  $50 - 500 \text{ cm}^{-1}$ , which is similar to the range of values used to calculate  $\omega_{pS}$  from the actual data for  $E \parallel c$  and  $E \perp c$  in  $\text{YBa}_2\text{Cu}_3\text{O}_{6+x}$  (as well as many other cuprate superconductors).

$T_c$ , a narrow peak due to unpaired carriers should be observed along the  $c$ -axis at (or below) microwave frequencies. Because a detailed knowledge exists for the temperature dependence of  $\lambda_c(T)$  as determined by microwave techniques,  $x_s^*/x_s$  and  $x_n$  can be determined for several temperatures, as shown in Table 1. The points in Fig. 6 show that with decreasing temperature  $x_n$  is decreasing and  $x_s^*/x_s$  is increasing in such a way as to suggest that, within the simple assumptions of Eq. (14),  $\Gamma_D$  is decreasing rapidly below  $T_c$ .

Taking the opposite extreme, if the damping is very large ( $\Gamma \approx \infty$ ), then the scattering time  $\tau \approx 0$  and the normal-fluid component will be incoherent. In this case, as Fig. 6 illustrates, the normal-fluid component has essentially no effect upon the calculated value of the condensate even for large values of  $x_n$ , and thus the optically-determined values of the condensate will be correct ( $x_s^* = x_s$ ). This is precisely the case along the  $c$ -axis in  $\text{YBa}_2\text{Cu}_3\text{O}_{6+x}$  for the oxygen ‘underdoped’ materials ( $x < 0.9$ ) where the behavior of the resistivity is ‘semiconducting’ [27], and the optical properties are characterized by the appearance of a pseudogap and the suppression of the low-frequency conductivity [12,28]. The estimates of the strength of the condensate along the  $c$ -axis in the underdoped  $\text{YBa}_2\text{Cu}_3\text{O}_{6.60}$  material determined by microwave ( $\omega_{pS} = 227 \pm 10 \text{ cm}^{-1}$ ) [26] and optical methods ( $\omega_{pS}^* = 244 \pm 20 \text{ cm}^{-1}$ ) [12] are in good agreement, as expected.

The final point that must be addressed is the effect that optical estimates of  $\omega_{pS}^*$  have on attempts to determine the temperature dependence of the penetration depth. As Fig. 7 shows, the temperature

Table 1

The plasma frequency of the condensate for  $\text{YBa}_2\text{Cu}_3\text{O}_{6.99}$  ( $T_c = 90 \text{ K}$ ) along the  $c$ -axis, as determined by optical (indicated by an asterisk) and by microwave techniques. Using a value for the Drude plasma frequency of  $\omega_{pD} = 2100 \text{ cm}^{-1}$ , the normal fluid fraction and the overestimate of the condensate have also been determined

$T$ (K)	$T/T_c$	[Optical] $\omega_{pS}^*$ ( $\text{cm}^{-1}$ )	[Microwave] $\omega_{pS}$ ( $\text{cm}^{-1}$ )	$x_n$	$x_s^*/x_s$
80	0.88	1310	995	0.78	1.73
60	0.67	1760	1290	0.61	1.86
40	0.44	1920	1395	0.55	1.89
10	0.11	2090	1450	0.52	2.07

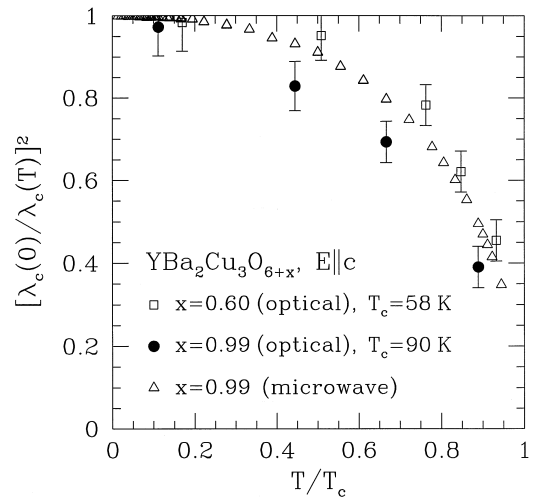


Fig. 7. A comparison of the optical estimates of  $[\lambda_c(0)/\lambda_c(T)]^2$  as a function of temperature for  $\text{YBa}_2\text{Cu}_3\text{O}_{6.60}$  (open squares) using a value of  $\lambda_c(0) = 6 \mu\text{m}$ , and  $\text{YBa}_2\text{Cu}_3\text{O}_{6.99}$  (solid circles) using  $\lambda_c(0) = 7520 \text{ \AA}$ . Microwave techniques have also been used to determine  $\lambda_c(T)$  using  $\lambda_c(0) = 11000 \text{ \AA}$  for the overdoped material (open triangles). The optical measurements on the overdoped material result in values which are lower than expected, as well as a strong temperature dependence at low temperature, due large number of unpaired carriers with a rapidly changing scattering rate below  $T_c$ .

dependence of  $[\lambda_c(0)/\lambda_c(T)]^2$  in the oxygen-underdoped  $\text{YBa}_2\text{Cu}_3\text{O}_{6.60}$  determined by optical techniques is very similar to that of  $\text{YBa}_2\text{Cu}_3\text{O}_{6.99}$  [26] as determined by microwave techniques. However, if the optical estimates for the condensate in the overdoped material are used, then a much stronger temperature dependence is observed at low temperature. This strong temperature dependence has also been observed in other optical experiments on overdoped systems [14]. This spurious behavior can be understood qualitatively in terms of the rapid formation of the condensate and the somewhat more gradual narrowing of the residual component. If the rapidly decreasing low-frequency conductivity in Fig. 1b is viewed as being due to the decrease in the scattering rate of the unpaired carriers, then we can conclude that  $\Gamma_D$  is large near  $T_c$ , and decreases for  $T \ll T_c$ . From Fig. 6, this implies that initially the optical estimates for the condensate are accurate. However, as the temperature is lowered and the condensate develops ( $x_n$  decreases) then the estimates for the condensate will be too large. As a result the optical

estimate for  $\lambda_c(0)$  ( $T \ll T_c$ ) will be too small and in general  $[\lambda_c(0)/\lambda_c(T)]^2$  will fall below the expected value, and the strong temperature dependence in the penetration depth is primarily due to the rapid narrowing of  $\Gamma_D$  in the presence of a large normal-state fraction. Note that in the underdoped case where it has been argued that the optical estimates of the condensate are accurate, the optical and microwave results for  $[\lambda_c(0)/\lambda_c(T)]^2$  are in good agreement [12].

#### 4. Conclusion

In the case of  $\text{YBa}_2\text{Cu}_3\text{O}_{6.99}$ , which is believed to be an anisotropic three dimensional metal ( $T \geq T_c$ ), and an unconventional superconductor ( $T < T_c$ ), there is a large amount of residual conductivity at low frequency due to carriers that have not collapsed into the  $\delta$  function. As a result, the strength of the condensate as determined by optical techniques is  $\omega_{\text{ps}}^* = 2090 \pm 70 \text{ cm}^{-1}$ , which is much larger than correct value determined from a microwave technique (which probes only the condensate) of  $\omega_{\text{ps}} = 1450 \pm 50 \text{ cm}^{-1}$ .

Using Eq. (7) the contribution of the condensate to  $\epsilon_1(\omega)$  may be removed, yielding the contribution due strictly to the unpaired carriers. The strong linear behavior of this residual component suggests that the damping  $\Gamma_D$  of the unpaired carriers at low temperature is very small, thus allowing the plasma frequency  $\omega_{\text{pN}} = 1450 \pm 50 \text{ cm}^{-1}$  to be determined. This yields a normal-state Drude plasma frequency of  $\omega_{\text{pD}} \approx 2100 \pm 70 \text{ cm}^{-1}$ , indicating that  $\approx 50\%$  of the free carriers have collapsed into the condensate, similar to what is observed in the *ab* plane. The lower value for  $\omega_{\text{pD}}$  removes the abrupt change in anisotropy above and below  $T_c$ , which had been observed in the past due to much larger values of  $\omega_{\text{pD}}$ .

In the underdoped  $\text{YBa}_2\text{Cu}_3\text{O}_{6+x}$  ( $x \lesssim 0.9$ ) materials, where the normal-state transport along the *c*-axis is ‘semiconducting’ (incoherent), optical estimates of the value of  $\omega_{\text{ps}}$  (and thus the penetration depth) are reliable and are in good agreement with microwave values. However, the large amount of residual conductivity in the overdoped material and the resulting overestimate in  $\omega_{\text{ps}}$ , will lead to serious

underestimates of  $\lambda_c(0)$ . Furthermore, the strong temperature dependence in optical determinations of  $[\lambda_c(0)/\lambda_c(T)]^2$  is most likely due to the rapidly changing values of  $x_n$  and  $\Gamma_D$  associated with the unpaired free carriers, whereas the actual temperature dependence below  $T_c/2$  is quite weak. There appears to be little variation in  $[\lambda_c(0)/\lambda(T)]^2$  along the *c*-axis for various values of oxygen dopings [29].

#### Acknowledgements

We would like to thank V.J. Emery, J.C. Irwin, A.J. Leggett, T. Timusk and R.J. Radtke for useful discussions. We would also like to acknowledge assistance in the laboratory from A.W. McConnell and Q. Song. This work was supported by the Natural Sciences and Engineering Research Council of Canada, Canadian Institute for Advanced Research, the Linville Institute, Simon Fraser University.

#### References

- [1] M. Tinkham, Introduction to Superconductivity, McGraw Hill, New York, 1975.
- [2] D.B. Tanner, T. Timusk, in: D.M. Ginsberg (Ed.), Physical Properties of High-Temperature Superconductors III, World Scientific, Singapore, 1992, p. 363.
- [3] S.L. Cooper, K.E. Gray, in: D.M. Ginsberg (Ed.), Physical Properties of High-Temperature Superconductors IV, World Scientific, Singapore, 1994, p. 61.
- [4] F. Wooten, Optical Properties of Solids, Academic Press, New York, 1972.
- [5] A.A. Abrikosov, L.P. Gor'kov, Sov. Phys. - JETP 12 (1960) 1243.
- [6] W.N. Hardy, D.A. Bonn, D.C. Morgan, R. Liang, K. Zhang, Phys. Rev. Lett. 70 (1993) 3999.
- [7] D.A. Bonn, R. Liang, T.M. Riseman, D.J. Baar, D.C. Morgan, K. Zhang, P. Dosanjh, T.L. Duty, A. MacFarlane, G.D. Morris, J.H. Brewer, W.N. Hardy, C. Kallin, A.J. Berlinsky, Phys. Rev. B 47 (1993) 11314.
- [8] Z.-X. Shen, D.S. Dessau, B.O. Wells, D.M. King, W.E. Spicer, A.J. Arko, D. Marshall, L.W. Lombardo, A. Kapitulnik, P. Dickinson, S. Doniach, J. Dicarolo, A.G. Loeser, C.H. Park, Phys. Rev. Lett. 70 (1993) 1553.
- [9] H. Ding, M.R. Norman, J.C. Campuzano, M. Randeria, A.F. Bellman, T. Yokoya, T. Takahashi, T. Mochiku, K. Kodowaki, Phys. Rev. B 54 (1996) R9678.
- [10] A. Puchkov, D.N. Basov, T. Timusk, J. Phys.-Condens. Matter 8 (1996) 10049.
- [11] K. Kamaraš, S.L. Herr, C.D. Porter, N. Tache, D.B. Tanner,

- S. Etemad, T. Venkatesan, E. Chase, A. Inam, X.D. Wu, M.S. Hegde, B. Dutta, *Phys. Rev. Lett.* 64 (1990) 84.
- [12] C.C. Homes, T. Timusk, D.A. Bonn, R. Liang, W.N. Hardy, *Physica C* 254 (1995) 265.
- [13] J. Schützmann, S. Tajima, S. Miyamoto, S. Tanaka, *Phys. Rev. Lett.* 73 (1994) 174.
- [14] J. Schützmann, S. Tajima, S. Miyamoto, Y. Sato, I. Terasaki, *Solid State Commun.* 94 (1995) 293.
- [15] R. Liang, P. Dosanjh, D.A. Bonn, D.J. Baar, J.F. Carolan, W.N. Hardy, *Physica C* 195 (1992) 51.
- [16] C.C. Homes, M. Reedyk, D.A. Crandles, T. Timusk, *Appl. Opt.* 32 (1993) 2972.
- [17] B. Koch, M. Dürrieler, H.P. Geserich, Th. Wolf, G. Roth, G. Zachmann, in: H. Kuzmany, M. Mehrig, J. Fink (Eds.), *Electronic Properties of High- $T_c$  Superconductors and Related Compounds*, Springer Series in Solid State Sciences, vol. 99, Springer, Berlin, 1990, p. 290.
- [18] H. Romberg, N. Nücker, J. Fink, Th. Wolf, X.X. Xi, B. Koch, H.P. Geserich, M. Dürrieler, W. Assmus, B. Gegenheimer, *Z. Phys. B-Condens. Matter* 78 (1990) 367.
- [19] D.A. Bonn, S. Kamal, K. Zhang, R. Liang, W.N. Hardy, *J. Phys. Chem. Solids* 56 (1995) 1941.
- [20] C.C. Homes, T. Timusk, D.A. Bonn, R. Liang, W.N. Hardy, *Can. J. Phys.* 73 (1995) 663.
- [21] C.J. Gorter, H.B.G. Casimir, *Z. Phys.* 35 (1943) 963.
- [22] S.L. Cooper, P. Nyhus, D. Reznik, M.V. Klein, W.C. Lee, D.M. Ginsberg, B.W. Veal, A.P. Paulikas, B. Dabrowski, *Phys. Rev. Lett.* 70 (1993) 1533.
- [23] S.L. Cooper, D. Reznik, A. Kotz, M.A. Karlow, R. Liu, M.V. Klein, W.C. Lee, J. Giapintzakis, D.M. Ginsberg, B.W. Veal, A.P. Paulikas, *Phys. Rev. B* 47 (1993) 8233.
- [24] D.N. Basov, R. Liang, D.A. Bonn, W.N. Hardy, B. Dabrowski, M. Quijada, D.B. Tanner, J.P. Rice, D.M. Ginsberg, T. Timusk, *Phys. Rev. Lett.* 74 (1995) 598.
- [25] J.L. Tallon, C. Bernhard, U. Binniger, A. Hofer, G.V.M. Williams, E.J. Ansaldo, J.I. Budnick, Ch. Niedermayer, *Phys. Rev. Lett.* 74 (1995) 1008.
- [26] S. Kamal, R. Liang, D.A. Bonn, W.N. Hardy, R. Liang, D.N. Basov, C.C. Homes, T. Timusk, unpublished.
- [27] T. Ito, Y. Kakamura, H. Takagi, S. Uchida, *Physica C* 185–189 (1991) 1267.
- [28] C.C. Homes, T. Timusk, D.A. Bonn, R. Liang, W.N. Hardy, *Phys. Rev. Lett.* 71 (1993) 1645.
- [29] D.A. Bonn, S. Kamal, A. Bonakdarpour, R. Liang, W.N. Hardy, C.C. Homes, D.N. Basov, T. Timusk, *Czech. J. Phys.* 46 (1996) 3195.